International Journal of Minerals, Metallurgy and Materials
Volume 29, Number 4, April 2022, Page 758
https://doi.org/10.1007/s12613-022-2425-4

Mathematical simulation of hot metal desulfurization during KR process coupled with an unreacted core model

Yanyu Zhao[1)], *Wei Chen*[2),✉], *Shusen Cheng*[1)], *and Lifeng Zhang*[3),✉]

1) School of Metallurgical and Ecological Engineering, University of Science and Technology Beijing, Beijing 100083, China
2) School of Mechanical Engineering, Yanshan University, Qinhuangdao 066004, China
3) School of Mechanical and Materials Engineering, North China University of Technology, Beijing 100144, China
(Received: 30 November 2021; revised: 13 January 2022; accepted: 24 January 2022)

Abstract: A three-dimensional mathematical model was established to predict the multiphase flow, motion and dispersion of desulfurizer particles, and desulfurization of hot metal during the Kanbara reactor (KR) process. The turbulent kinetic energy–turbulent dissipation rate (k–ε) turbulence model, volume-of-fluid multiphase model, discrete-phase model, and unreacted core model for the reaction between the hot metal and particles were coupled. The measured sulfur content of the hot metal with time during the actual KR process was employed to validate the current mathematical model. The distance from the lowest point of the liquid level to the bottom of the ladle decreased from 3170 to 2191 mm when the rotation speed increased from 30 to 110 r/min, which had a great effect on the dispersion of desulfurizer particles. The critical rotation speed for the vortex to reach the upper edge of the stirring impeller was 70 r/min when the immersion depth was 1500 mm. The desulfurization rate increased with the increase in the impeller rotation speed, whereas the influence of the immersion depth was relatively small. Formulas for different rotation parameters on the desulfurization rate constant and turbulent energy dissipation rate were proposed to evaluate the variation in sulfur content over time.

Keywords: desulfurization; unreacted core model; desulfurizer dispersion; KR process; fluid flow

1. Introduction

Excessive sulfur content seriously affects the processing performance of steel [1–2]. Therefore, the Kanbara reactor (KR) hot-metal pretreatment process is widely used as an effective desulfurization method, which was first developed by Nippon Steel as early as 1965 [3–4]. A large number of studies have investigated the flowing fluid and desulfurizer distribution through physical modeling [5–8] and numerical simulation [9–13]. Visuri *et al.* [14] presented a comprehensive review on hot-metal desulfurization, including the fluid flow, bath mixing, and particle dispersion. He *et al.* [11] used the Eulerian–Lagrangian approach to investigate the distribution and motion behavior of desulfurizer particles influenced by the flow field and summarized four typical motion trajectories of desulfurizer particles. Wang *et al.* [12] built a transient-coupled three-dimensional (3D) numerical model to investigate the two-phase flow, heat transfer, and particle motion during KR desulfurization processes. The aggregation of desulfurizer particles was considered. Lee and Yi [15] developed a new impeller profile to improve the desulfurization efficiency of the KR process using operational data analysis and numerical simulation.

The methods used to study hot-metal desulfurization can be divided into laboratory experiments and industrial trials [16–17], mathematical simulation [12,18], and data driven analysis [19]. Lindström and Du [16] and Mitsuo *et al.* [17] obtained the change in thickness of the desulfurization product over time through experiments. Oeters [20] established a model to calculate the desulfurization reaction considering the boundary layer diffusion. Nakanishi *et al.* [21] proposed a method to calculate the mass transfer rate, which is related to the velocity of particles and hot metal. Previous studies have focused on the overall desulfurization rate. However, the desulfurization effect of each desulfurizer in the hot metal is in line with the process of adding desulfurizer particles for desulfurization. Thus, in the current study, a 3D mathematical model coupled with the turbulent kinetic energy-turbulent dissipation rate (k–ε) model, volume-of-fluid (VOF) multiphase model, discrete-phase model (DPM), and unreacted core model were established to predict desulfurization during the KR process.

2. Mathematical formulation

2.1. Computational domain

The KR desulfurization process in an industrial trial using 250 t hot metal ladle was numerically studied. Fig. 1 shows the 3D computational domain and grid system. The upper radius, lower radius, and height of the hot metal ladle were

✉ Corresponding authors: Wei Chen E-mail: weichen@ysu.edu.cn; Lifeng Zhang E-mail: zhanglifeng@ncut.edu.cn

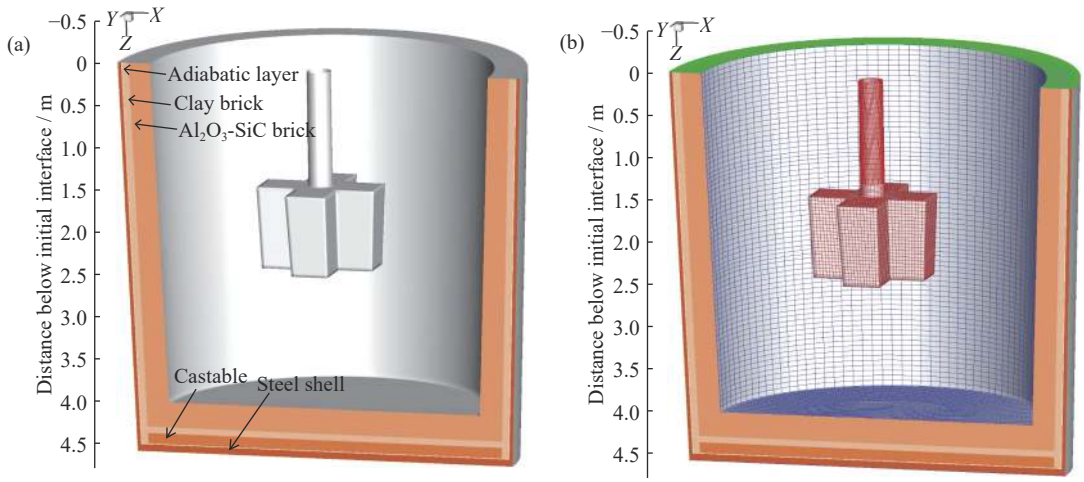

Fig. 1. Schematic of the hot metal ladle (a) and grid system (b).

2418, 2254, and 4571 mm, respectively. The height of the liquid level was 3184 mm after 250 t of the hot metal was loaded. The ladle lining was mainly composed of Al_2O_3–SiC brick, clay brick, castable, adiabatic layer, and steel shell. A commonly used cross-shaped impeller with a height of 950 mm and rotation diameter of 1400 mm was employed. The entire computational domain was divided into approximately 780000 structured grids. Table 1 summarizes the detailed model parameters. The effect of rotation speed and immersion depth of the impeller on the multiphase flow and desulfurization was proposed.

Table 1. Dimensions and physical parameters

Parameter	Value	Parameter	Value
Impeller height / mm	950	Rotation speed / (r·min^{-1})	30, 40, 50, 60, 70, 80, 90, 100, 110
Impeller rotation diameter / mm	1400	Immersion depth / mm	1500, 1600, 1700
Shaft diameter / mm	280	Initial sulfur content / wt%	0.040
Al_2O_3–SiC brick thickness / mm	255 in radial, 295 in axial	Hot metal density / (kg·m^{-3})	6700
Clay brick / mm	80 in radial, 75 in axial	Hot metal viscosity / (kg·m^{-1}·s^{-1})	6.486×10^{-3}
Castable / mm	125	Air density / (kg·m^{-3})	1.225
Adiabatic layer / mm	10	Air viscosity / (kg·m^{-1}·s^{-1})	1.789×10^{-5}
Steel shell / mm	40 in radial, 80 in axial	Surface tension / (N·m^{-1})	1.6

2.2. Governing equation

The hot metal and air phase were considered to be continuous phases in the current study. The VOF multiphase model was used to resolve the interface between different phases. For the q phase, the continuity equation is described as follows:

$$\frac{\partial}{\partial t}\left(\alpha_q \rho_q\right) + \nabla \cdot \left(\alpha_q \rho_q \boldsymbol{u}_q\right) = 0 \tag{1}$$

$$\sum_{q=1}^{m} \alpha_q = 1 \tag{2}$$

where α_q is the volume fraction of q phase; $\boldsymbol{u}_q$ is the velocity of q phase, m/s; ρ_q is the density of q phase, kg/m^3; t is the calculation time, s; m is the total number of the continuous phases.

The momentum equation is calculated as follows:

$$\frac{\partial}{\partial t}(\rho \boldsymbol{u}) + \nabla \cdot (\rho \boldsymbol{u}\boldsymbol{u}) = -\nabla P + \nabla \cdot \left[\mu\left(\nabla \boldsymbol{u} + \nabla \boldsymbol{u}^{\mathrm{T}}\right)\right] + \rho \boldsymbol{g} + \boldsymbol{F} \tag{3}$$

where ρ is the density of the mixture phase, kg/m^3; $\boldsymbol{u}$ is the velocity, m/s; μ is viscosity of the mixture phase, kg/(m·s); P is the pressure, Pa; $\boldsymbol{F}$ is the source term, kg/(m^2·s^2).

The standard k–ε model was employed to calculate the turbulent parameters. The turbulent kinetic energy k and turbulent dissipation rate ε were respectively calculated as follows:

$$\alpha_1 \rho_1 \left(\frac{\partial k}{\partial t} + \frac{\partial (k u_i)}{\partial x_i}\right) = \frac{\partial}{\partial x_j}\left[\alpha_1 \left(\mu + \frac{\mu_t}{\sigma_k}\right)\frac{\partial k}{\partial x_j}\right] + \alpha_1 G_k - \alpha_1 \rho_1 \varepsilon \tag{4}$$

$$\alpha_1 \rho_1 \left(\frac{\partial \varepsilon}{\partial t} + \frac{\partial \varepsilon u_i}{\partial x_i}\right) = \frac{\partial}{\partial x_j}\left[\alpha_1 \left(\mu + \frac{\mu_t}{\sigma_\varepsilon}\right)\frac{\partial \varepsilon}{\partial x_j}\right] + \alpha_1 C_{1\varepsilon}\frac{\varepsilon}{k} G_k - \alpha_1 C_{2\varepsilon} \rho_1 \frac{\varepsilon^2}{k} \tag{5}$$

where α_1 is the volume fraction of hot metal; ρ_1 is the density of hot metal, kg/m^3; u_i is the velocity in i direction, m/s; x_i and x_j is the coordinate in i direction and j direction in m, respectively; μ_t is the turbulent viscosity, kg/(m·s); G_k is the generation of turbulence kinetic energy due to the mean velocity gradients, kg/(m·s^3); σ_k and σ_ε are the turbulent Prandtl numbers for k and ε, respectively; $C_{1\varepsilon}$ and $C_{2\varepsilon}$ are constants; the value of constants are $C_{1\varepsilon} = 1.44$, $C_{2\varepsilon} = 1.92$, $\sigma_k = 1.0$, and $\sigma_\varepsilon = 1.3$.

The CaO desulfurizer was considered as a discrete phase, and the trajectory was calculated by integrating the following

equation [22–25]:

$$\frac{\mathrm{d}\boldsymbol{u}_\mathrm{p}}{\mathrm{d}t}=\frac{(\rho_\mathrm{p}-\rho_\mathrm{l})}{\rho_\mathrm{p}}\boldsymbol{g}+\frac{3\mu_\mathrm{l}C_\mathrm{D}Re}{4\rho_\mathrm{p}d_\mathrm{p}^2}\left(\boldsymbol{u}_\mathrm{l}-\boldsymbol{u}_\mathrm{p}\right)+C_\mathrm{VM}\frac{\rho_\mathrm{l}}{\rho_\mathrm{p}}\frac{\mathrm{d}}{\mathrm{d}t}\left(\boldsymbol{u}_\mathrm{l}-\boldsymbol{u}_\mathrm{p}\right)+\frac{\rho_\mathrm{l}}{\rho_\mathrm{p}}\boldsymbol{u}_\mathrm{p}\nabla\cdot\boldsymbol{u}_\mathrm{l} \quad (6)$$

where the four terms on the right side of the equation are gravity buoyancy force, drag force, pressure gradient force, and virtual mass force, respectively. $\boldsymbol{u}_\mathrm{p}$ and $\boldsymbol{u}_\mathrm{l}$ is the velocity of the CaO desulfurizer and hot metal in m/s, respectively; ρ_p and ρ_l is the density of the CaO desulfurizer and hot metal in kg/m^3, respectively; C_D is the drag force coefficient; Re is the Reynolds number; d_p is the diameter of the CaO desulfurizer, m; C_VM is the virtual mass force coefficient; The detailed parameters of these forces can be found in previous studies [22–25].

A user-defined scalar (UDS) transport equation, which is defined as follows, was used in the convection and diffusion of sulfur in the hot metal:

$$\frac{\partial}{\partial t}(\rho C_\mathrm{S})+\nabla\cdot(\rho\boldsymbol{u}C_\mathrm{S})=\nabla\cdot\left(\left(\rho D_\mathrm{S}+\frac{\mu_\mathrm{t}}{Sc_\mathrm{t}}\right)\nabla\cdot C_\mathrm{S}\right)+S_\mathrm{CaO} \quad (7)$$

where C_S is the mass fraction of sulfur in the hot metal; D_S is the diffusion coefficient of sulfur in m^2/s; Sc_t is the turbulent Schmidt number; S_CaO is the desulfurization source induced by the CaO desulfurizer, kg/(m^3·s).

2.3. Desulfurization kinetic model

Sulfur was absorbed by the CaO desulfurizer due to a chemical reaction (Eq. (8)):

$$(\mathrm{CaO})+[\mathrm{S}]=(\mathrm{CaS})+[\mathrm{O}] \quad (8)$$

The unreacted core model was used to solve the kinetic process of desulfurization. The particle size was assumed to remain unchanged and the core to be unreactive. However, the reaction interface continuously advanced toward the core during desulfurization (Fig. 2).

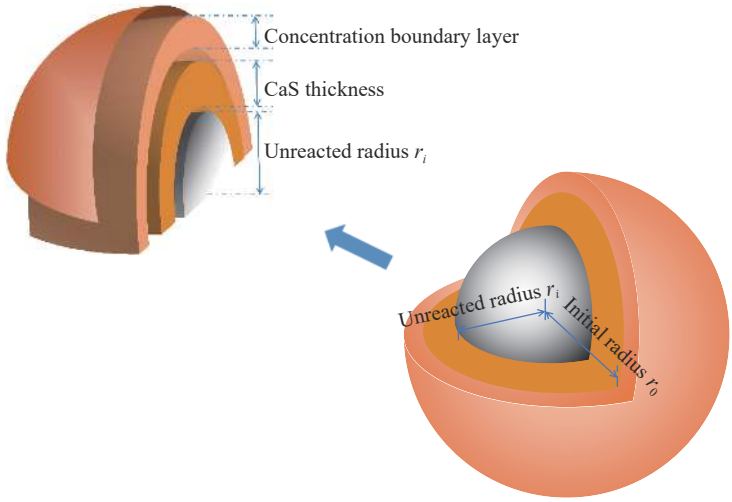

Fig. 2. Schematic of the unreacted core model.

Oeters *et al.* [26] indicated that the boundary layer diffusion forms the rate limiting step at sulfur contents of less than 0.05wt%. Thus, the desulfurization rate V_S and desulfurization source S_{CaO} were respectively calculated as follows:

$$V_\mathrm{S}=4\pi r_0^2\rho_\mathrm{l}k_\mathrm{g}(C_\mathrm{S}-C_\mathrm{Se}) \quad (9)$$

$$S_\mathrm{CaO}=V_\mathrm{S}/V=\frac{4\pi r_0^2\rho_\mathrm{l}k_\mathrm{g}(C_\mathrm{S}-C_\mathrm{Se})}{V} \quad (10)$$

where V_S is the desulfurization rate, kg/s; V is the volume of the grid where the particle was located, m^3; r_0 is the initial radius of the CaO desulfurizer; ρ_l is the density of the hot metal, kg/m^3; C_S is the mass fraction of sulfur; C_Se is the equilibrium mass fraction of sulfur and assumed as 0 [4]. The mass transfer coefficient k_g is defined in Eq. (11) (m/s).

$$k_\mathrm{g}=\frac{D_\mathrm{S}}{d_\mathrm{p}}\left(2.0+0.6Re^{1/2}Sc^{1/3}\right) \quad (11)$$

$$Re=\frac{\rho d_\mathrm{p}\left|\boldsymbol{u}_\mathrm{p}-\boldsymbol{u}_\mathrm{l}\right|}{\mu} \quad (12)$$

$$Sc=\frac{\mu}{\rho D_\mathrm{S}} \quad (13)$$

where D_S is the diffusion coefficient of sulfur and set as 2.8×10^{-8} m^2/s [27], d_p is the diameter of the CaO desulfurizer, Re is the local Reynolds number, and Sc is the Schmidt number.

The diffusion rate of sulfur through the concentration boundary layer was equal to the consumption rate of CaO at the unreacted interface. Therefore, the reaction time t has the following relationship with the radius of the unreacted r_i:

$$-\frac{4\pi r_i^2\rho_\mathrm{CaO}}{M_\mathrm{CaO}}\frac{\mathrm{d}r_i}{\mathrm{d}t}=4\pi r_0^2k_\mathrm{g}\left(\frac{C_\mathrm{S}\rho_\mathrm{l}}{M_\mathrm{S}}-\frac{C_\mathrm{Se}\rho_\mathrm{l}}{M_\mathrm{S}}\right) \quad (14)$$

where ρ_CaO is the density of CaO, kg/m^3; M_CaO and M_S are the molar mass of CaO and sulfur, respectively. The following relationship can be obtained after integrating Eq. (14):

$$t=\frac{M_\mathrm{S}\rho_\mathrm{CaO}r_0}{3M_\mathrm{CaO}\rho_\mathrm{l}k_\mathrm{g}(C_\mathrm{S}-C_\mathrm{Se})}\left[1-\left(\frac{r_i}{r_0}\right)^3\right] \quad (15)$$

2.4. Boundary conditions

The stirring of the impeller was achieved using the multiple-reference frame model [12]. Thus, the computation domain was divided into a moving reference frame containing the stirring impeller and a stationary reference frame contain-

ing the rest. The standard k–ε model, VOF model, DPM, and UDS equation were integrated using the commercial ANSYS FLUENT 17.0 software. A pressure outlet boundary was used at the top of the ladle. The moving no-slip wall was adopted for the impeller and shaft wall. The remaining walls were set as no-slip boundary conditions. The amount of CaO desulfurizer was 1378 kg, and the adding time was 60 s. The adding position was 1.8 m above the liquid level and 1/2 radius from the axis. The density of CaO particles was 3320 kg/m^3, and the density was assumed constant during the desulfurization process. The diameter distribution of the actual CaO particles was measured through a sifter. The specific results are shown in Table 2. The Pressure-Implicit with Splitting of Operators (PISO) scheme was used for the pressure–velocity coupling, and the second-order upwind was used for discretization. The time step size was 0.005 s, and the total time for each case was over 700 s to reach a steady state.

Table 2. Diameter and mass fraction of the CaO desulfurizer

Diameter / mm	Mass fraction
0.2	0.24
0.4	0.23
0.6	0.104
0.8	0.108
1.0	0.15
2.0	0.168

3. Distribution of multiphase flow and surface level

Fig. 3 shows the effect of impeller rotation speed on the distribution of the streamline with 1500 mm immersion depth. The liquid level presented a funnel shape, and the lowest point of the liquid level reached the upper edge of the stirring impeller when the rotation speed was 70 r/min. The molten iron in the ladle moved violently, and a large amount of air was entrained into the hot metal when the speed was 110 r/min. Fig. 4 shows the effect of rotation speed on the average volume of the turbulent energy dissipation rate, presenting a law of increase with the increase in rotation speed. Eq. (16) provides the regression formula:

$$\varepsilon_{ave} = 2.6421 \times 10^{-6} \cdot n^{2.7468} \quad (16)$$

where ε_{ave} is the average turbulent energy dissipation rate, m^2/s^3; n is the rotation speed, r/min. The distance from the lowest point of the liquid level to the bottom of the ladle decreased from 3170 to 2191 mm when the rotation speed increased from 30 to 110 r/min. The critical rotation speed at which the lowest point of the liquid level reached the upper edge of the stirring impeller was 70 r/min when the immersion depth was 1500 mm. In addition, when the rotation speed was increased to 110 r/min, a dead zone remained at the bottom of the stirring impeller, which resulted in a low desulfurization rate.

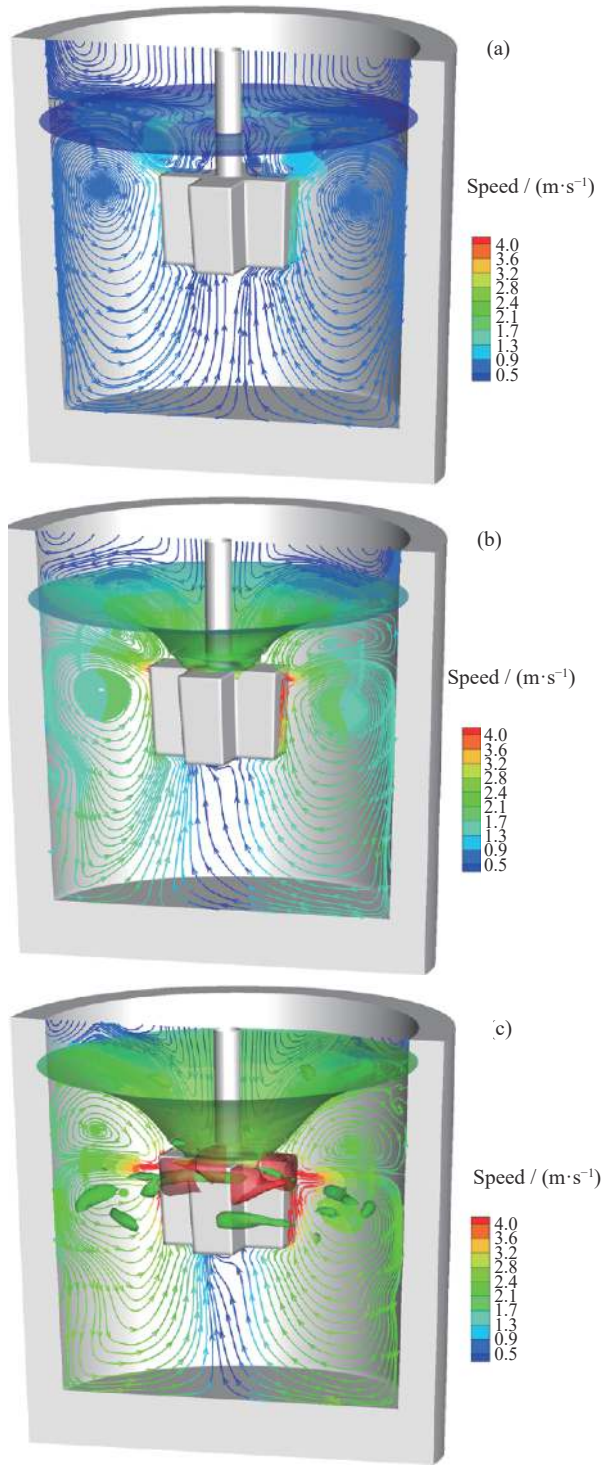

Fig. 3. Effect of rotation speed on the distribution of the streamline and liquid level with 1500 mm immersion depth at (a) 30, (b) 70, and (c) 110 r/min.

4. Dispersion of desulfurizers in hot metal

Fig. 5 shows the variation in the sulfur content and spatial distribution of CaO desulfurizers over time at a 110 r/min rotation speed and 1500 mm immersion depth. The sulfur content gradually decreased due to the absorption of CaO desulfurizer. The sulfur content can be reduced to less than 0.001wt% after stirring for 600 s under current conditions, and it was relatively uniformly distributed in the entire hot

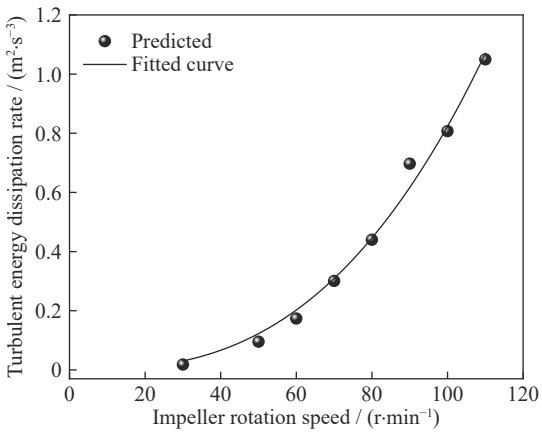

Fig. 4. Effect of rotation speed on the average turbulent energy dissipation rate with 1500 mm immersion depth.

metal because of the high stirring speed. Fig. 6 shows four typical 3D trajectories of CaO desulfurizers, including rotation in the dead zone at the bottom of the stirring impeller, dispersion in the hot metal after being hit by the stirring impeller, rotation in the core area of stirring, and rotation in the relatively weak stirring areas. More CaO desulfurizer should be dispersed by the hitting of the stirring impeller to obtain a good dispersion degree and high utilization of the desulfurizer.

The lowest point of the liquid level mentioned above had a significant influence on the desulfurization efficiency. This point can indirectly reflect the dispersion of the desulfurizer in the hot metal ladle. Fig. 7 shows the concentration distribution of the CaO desulfurizer under three typical conditions. The particle dispersion was low at the 30 r/min rotation speed. The vast majority of CaO desulfurizers accumulated at the hot metal-air interface under the action of buoyancy. Given that the CaO desulfurizer had a certain initial speed when it was immersed in the hot metal, a part of it was dispersed at a low rotation speed. The dispersion degree of CaO desulfurizers increased with the increase in rotation speed. The floating CaO desulfurizers were re-injected into the hot metal under the action of the stirring impeller when the lowest point of the liquid level reached the stirring impeller, which improved the dispersion of the desulfurizer and increased the desulfurization efficiency.

5. Effect of process parameters on desulfurization

The sulfur content at different times in an actual KR desulfurization industrial trial was analyzed to validate the current mathematical model (Fig. 8). The rotation and immer-

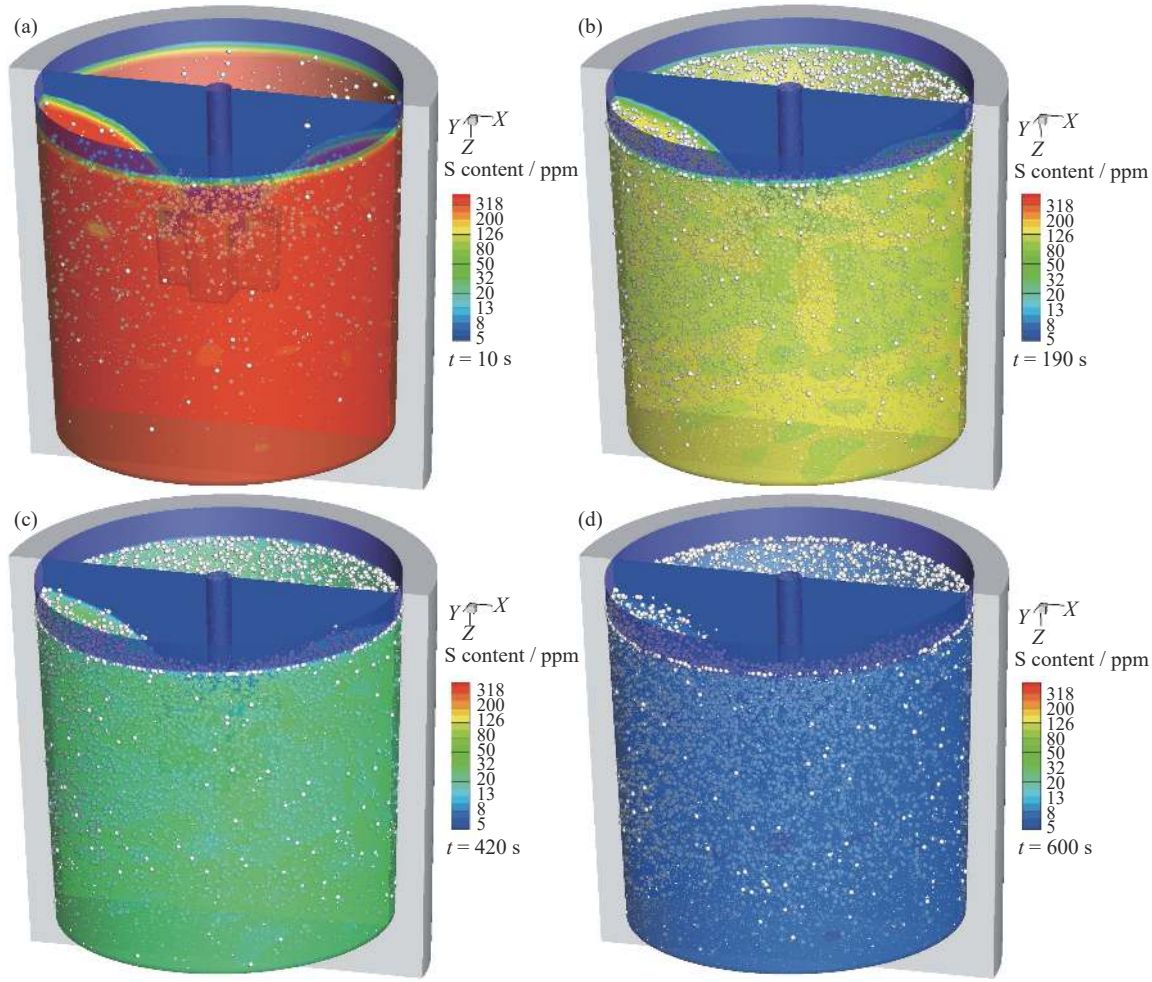

Fig. 5. Variation in the sulfur content and spatial distribution of CaO desulfurizers over time at a 110 r/min rotation speed and 1500 mm immersion depth: (a) 10, (b) 190, (c) 420, and (d) 600 s.

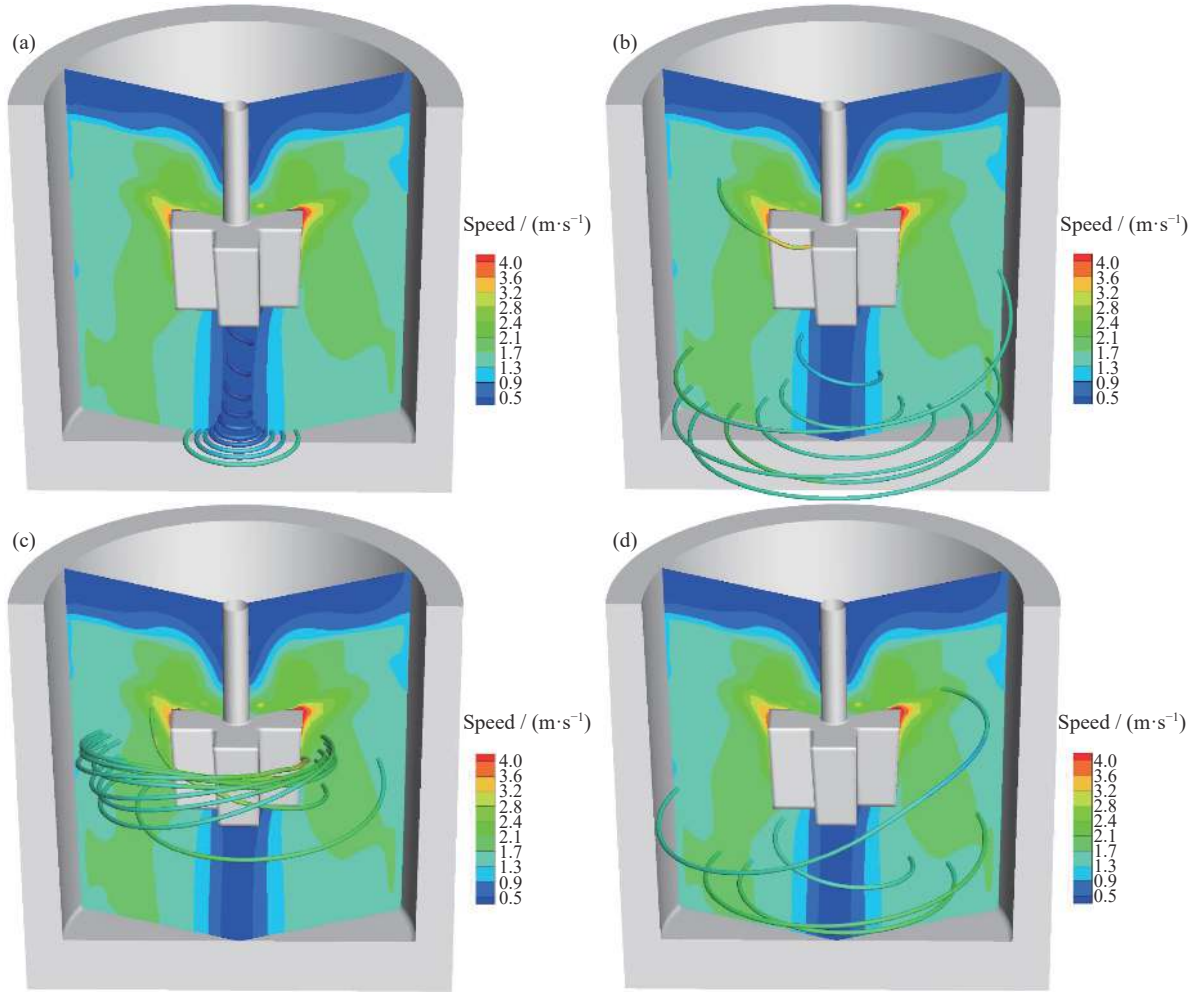

Fig. 6. Four typical 3D trajectories of CaO desulfurizers: (a) rotation in the dead zone at the bottom of the stirring impeller; (b) dispersion in the hot metal after being hit by the stirring impeller; (c) rotation in the core area of stirring; (d) rotation in the relatively weak stirring areas.

sion depth of the impeller were 90 r/min and 1500 mm, respectively. The initial sulfur content was 0.04wt%, and the parameter of the desulfurizer is shown in Table 2. The predicted sulfur content was in good agreement with the measured value. Therefore, the current model can accurately predict the change in sulfur content over time.

Fig. 9 shows the effect of rotation speed on the average sulfur content and average desulfurization rate with 1500 mm immersion depth. The desulfurization rate gradually increased with the increase in impeller rotation speed. The increase in rotation speed led to an increased degree of dispersion of the desulfurizer and speed of the hot metal. The desulfurization rate increased significantly during the adding time of the desulfurizer. The desulfurization rate constant at 110 r/min was about three times that at 30 r/min at the end of the adding process. In the subsequent process, the sulfur content gradually decreased, and the driving force for desulfurization decreased, which caused a decrease in the desulfurization rate. The increase in desulfurization rate gradually decreased when the rotation speed was greater than 80 r/min. The increase in rotation speed had a limited effect on the degree of dispersion of the desulfurizer after the lowest point of the liquid level reached the stirring impeller.

Fig. 10 shows the effect of impeller immersion depth on the sulfur content at different rotation speeds. As the immersion depth increased, the desulfurization rate increased slightly. However, with the increase in rotation speed, the amplitude of the increase gradually decreased. This finding indicated that the current limited immersion depth adjustment range hardly affected the desulfurization efficiency during the actual KR process.

The desulfurization reaction was assumed to follow the first-order reaction law [4,28–29]. Thus, the change in sulfur content with time can be calculated as Eq. (17):

$$-\frac{\mathrm{d}[\%\mathrm{S}]}{\mathrm{d}t} = \beta \cdot [\%\mathrm{S}] \tag{17}$$

where β is the desulfurization rate constant, s^{-1}; t is the reaction time, s. Integrating Eq. (17) and assuming that the equilibrium sulfur content is 0 [4], the following can be obtained:

$$[\%\mathrm{S}] = [\%\mathrm{S}]_0 \cdot \mathrm{e}^{-\beta t} \tag{18}$$

where $[\%S]_0$ is the initial sulfur content.

Therefore, the variation in sulfur content with time can be estimated by solving the desulfurization rate constant β. The

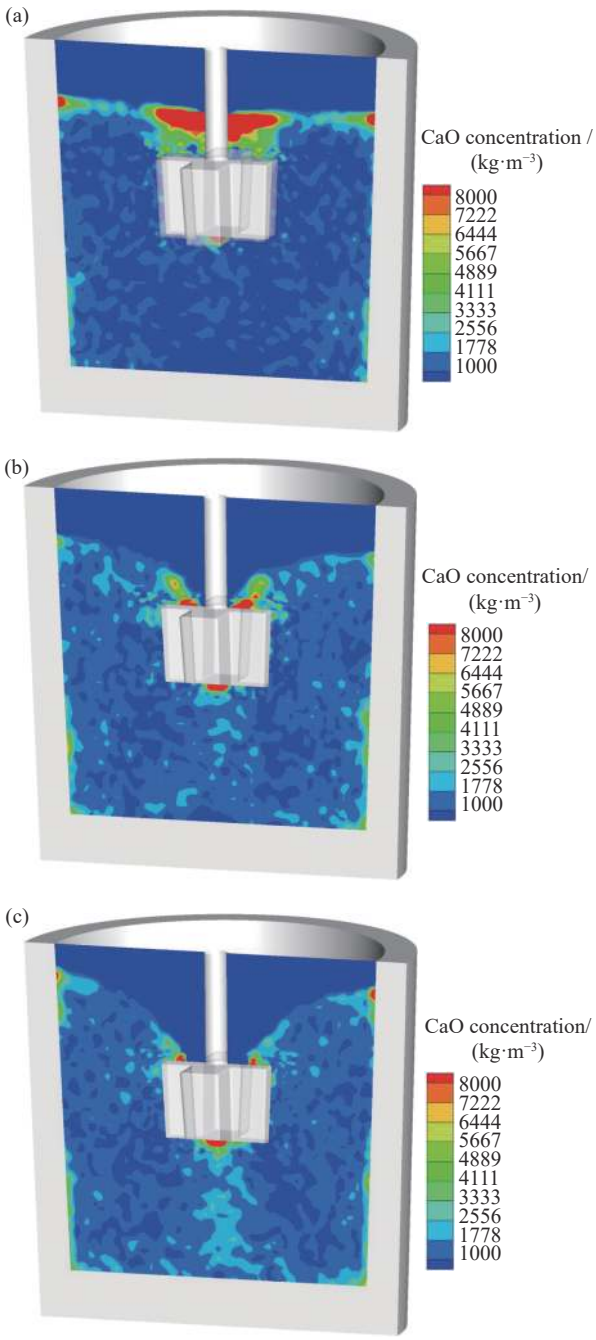

Fig. 7. Effect of rotation speed on the distribution of desulfurizer concentration with 1500 mm immersion depth at (a) 30, (b) 70, and (c) 110 r/min.

desulfurization rate constant β can be calculated by fitting the results after adding the desulfurizer (Fig. 9). The impeller rotation speed mainly changed the desulfurization efficiency by changing the stirring power of the hot metal. Thus, the relationship between the desulfurization rate constant β and turbulent energy dissipation rate ε (Fig. 11) was determined based on the results in Figs. 4 and 9. The desulfurization rate constant increased with the increase in turbulent energy dissipation rate. The relationship between the sulfur content and turbulent energy dissipation rate can be obtained by substituting the fitted $\beta = 0.00688 \cdot \varepsilon^{0.265}$ into Eq. (18).

$$[\%S] = [\%S]_0 \cdot e^{-0.00688 \cdot \varepsilon^{0.265} \cdot t} \tag{19}$$

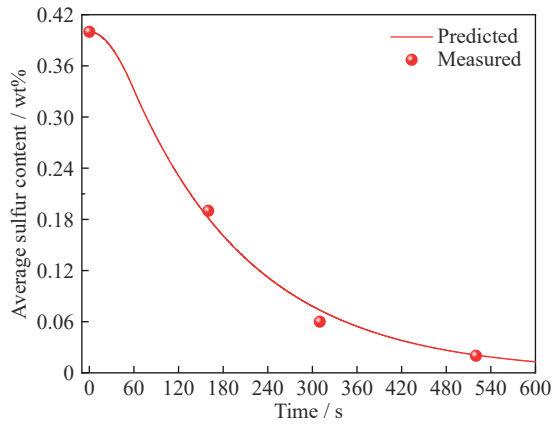

Fig. 8. Comparison of the measured and predicted sulfur contents.

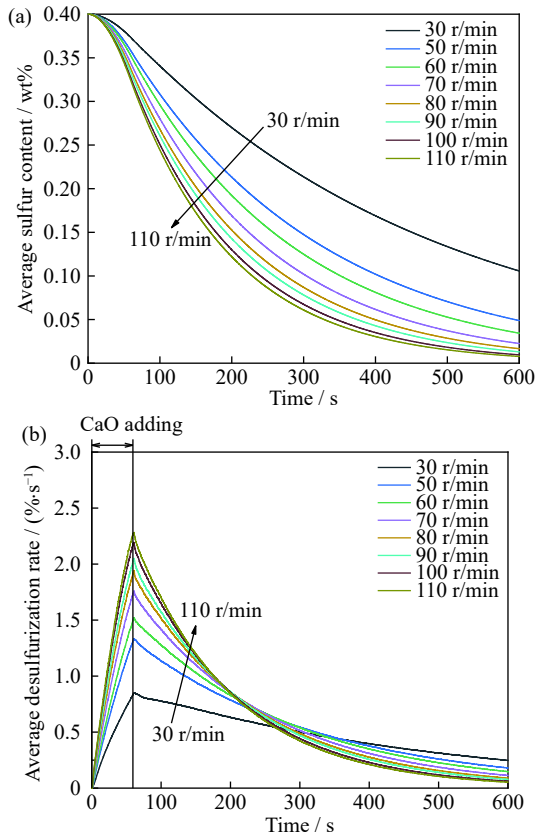

Fig. 9. Effect of rotation speed on the average sulfur content (a) and average reaction rate of desulfurization (b) with 1500 mm immersion depth.

Fig. 11 compares the effect of stirring methods [29] and ladle capacities [4] on the relationship between the desulfurization rate constant and turbulent energy dissipation rate. The results of the 70 kg ladle desulfurization experiment conducted by Nakai *et al.* [4] were consistent with the trend of the current model, thus proving the correctness of the model. Moreover, the effect of mechanical stirring was better than that of gas stirring. The determined relationship in Eq. (19) can be used to evaluate the stirring time required for desulfurization from the initial content to 0.005wt% under different rotation parameters, which is important in the industrial production cycle.

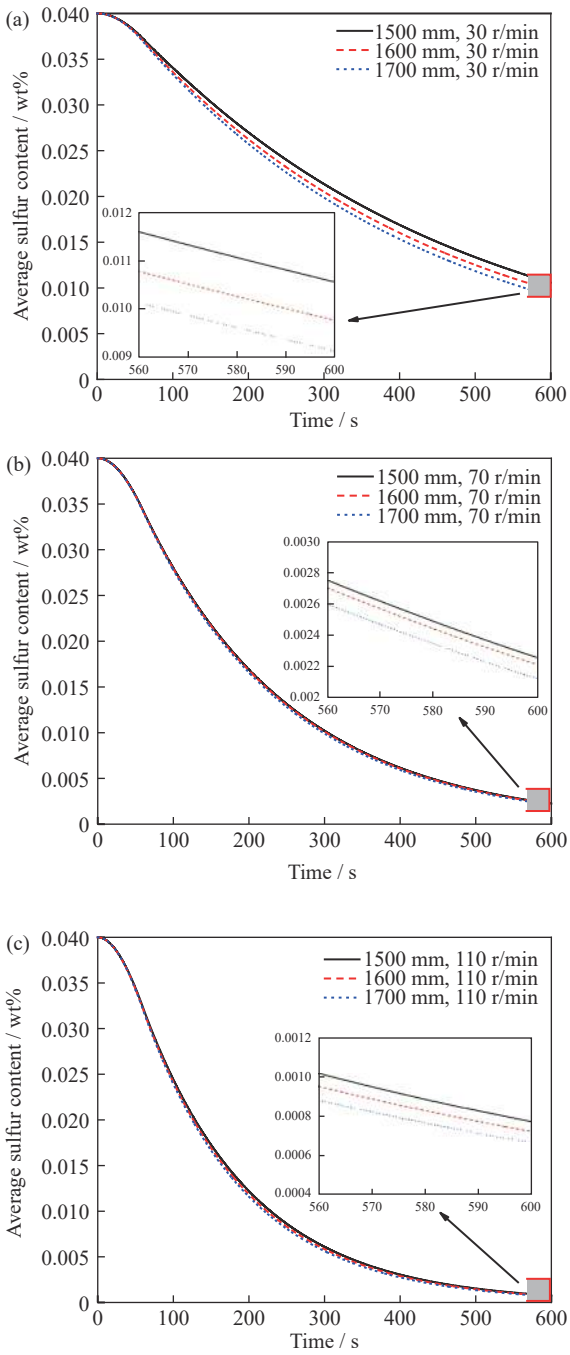

Fig. 10. Effect of impeller immersion depth on sulfur content at different rotation speeds: (a) 30, (b) 70, and (c) 110 r/min.

6. Conclusion

In summary, the current 3D mathematical model, coupled with the k–ε model, VOF multiphase model, DPM, and unreacted core model, was successfully used to predict the multiphase flow, motion and dispersion of desulfurizer particles, and desulfurization of hot metal during the KR process. The main conclusions obtained were as follows.

(1) The flow field and turbulent energy dissipation rate of the hot metal increased with the increase in impeller rotation speed. The regression formula between the impeller rotation speed and turbulent energy dissipation rate was proposed.

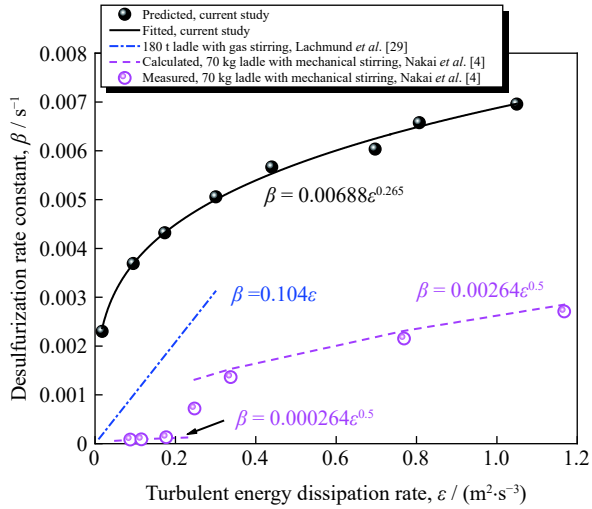

Fig. 11. Relationship between the rate constant β and turbulent energy dissipation rate ε for the desulfurization of KR industrial and pilot-scale trials.

The distance from the lowest point of the liquid level to the bottom of the ladle decreased from 3170 to 2191 mm when the rotation speed increased from 30 to 110 r/min. The critical rotation speed at which the lowest point of the liquid level reached the upper edge of the stirring impeller was 70 r/min when the immersion depth was 1500 mm.

(2) Four typical trajectories of CaO desulfurizers were predicted, including rotation in the dead zone at the bottom of the stirring impeller, dispersion in the hot metal after being hit by the stirring impeller, rotation in the core area of stirring, and rotation in the relatively weak stirring areas. Desulfurization mainly occurred at the surface of the desulfurizer moving in the hot metal. Therefore, the ratio of desulfurizer re-injected into the hot metal must be increased by the stirring impeller as much as possible to improve the utilization rate of the desulfurizer.

(3) The desulfurization rate increased with the increase in impeller rotation speed, and the influence of the immersion depth was relatively small. The desulfurization rate increased significantly when the rotation speed increased from 30 to 90 r/min, whereas the subsequent increase in desulfurization rate was smaller with the increase in rotation speed. The average sulfur content presented an exponential function with time. The desulfurization rate gradually decreased with time after the desulfurizer was added, and the greater the rotation speed, the faster the decrease in desulfurization rate.

(4) The desulfurization rate constant at 110 r/min was about three times that at 30 r/min at the end of the adding of desulfurizers. An exponential function relationship was observed between the turbulent kinetic energy dissipation rate ε and the desulfurization rate constant β, and the fitting relationship was $\beta = 0.00688 \cdot \varepsilon^{0.265}$. Formulas for different rotation parameters on the desulfurization rate constant and turbulent energy dissipation rate were proposed to evaluate the variation in sulfur content over time and provide theoretical guidance for industrial production.

Acknowledgements

This work was financially supported by the National Science Foundation China (No. 52104343), the Natural Science Foundation of Hebei Province, China (No. E2021203222). The authors are grateful for the support from the High Steel Center (HSC) at Yanshan University and North China University of Technology, China.

Conflict of Interest

On behalf of all authors, the corresponding author states that there is no conflict of interest.

References

[1] L. Lin and J.Q. Zeng, Consideration of green intelligent steel processes and narrow window stability control technology on steel quality, *Int. J. Miner. Metall. Mater.*, 28(2021), No. 8, p. 1264.

[2] C.B. Shi, Y. Huang, J.X. Zhang, J. Li, and X. Zheng, Review on desulfurization in electroslag remelting, *Int. J. Miner. Metall. Mater.*, 28(2021), No. 1, p. 18.

[3] K. Kanbara, T. Nisugi, and O. Shiraishi, Desulfurization process using mechanical impeller, *Tetsu-to-Hagané*, 58(1972), No. 4, p. S26.

[4] Y. Nakai, I. Sumi, H. Matsuno, N. Kikuchi, and Y. Kishimoto, Effect of flux dispersion behavior on desulfurization of hot metal, *ISIJ Int.*, 50(2010), No. 3, p. 403.

[5] Y. Liu, M. Sano, T.A. Zhang, Q. Wang, and J.C. He, Intensification of bubble disintegration and dispersion by mechanical stirring in gas injection refining, *ISIJ Int.*, 49(2009), No. 1, p. 17.

[6] S. Horiuchi, M.A. Uddin, Y. Kato, Y. Takahashi, and Y.I. Uchida, Mass transfer between different phases in a mechanically-stirred vessel and its comparison with that in a gas-stirred one, *ISIJ Int.*, 54(2014), No. 1, p. 87.

[7] Y. Nakai, Y. Hino, I. Sumi, N. Kikuchi, Y. Uchida, and Y. Miki, Effect of flux addition method on hot metal desulfurization by mechanical stirring process, *ISIJ Int.*, 55(2015), No. 7, p. 1398.

[8] M. Li, Y.B. Tan, J.L. Sun, D. Xie, and Z. Liu, Drawdown mechanism of light particles in baffled stirred tank for the KR desulphurization process, *Chin. J. Chem. Eng.*, 27(2019), No. 2, p. 247.

[9] Y. Nakai, I. Sumi, N. Kikuchi, K. Tanaka, and Y. Miki, Powder blasting in hot metal desulfurization by mechanical stirring process, *ISIJ Int.*, 57(2017), No. 6, p. 1029.

[10] Y. Liu, Z.M. Zhang, S. Masamichi, J. Zhang, P. Shao, and T.A. Zhang, Improvement of impeler blade structure for gas injection refining under mechanical stirring, *J. Iron Steel Res. Int.*, 21(2014), No. 2, p. 135.

[11] M.L. He, N. Wang, M. Chen, M. Chen, and C.F. Li, Distribution and motion behavior of desulfurizer particles in hot metal with mechanical stirring, *Powder Technol.*, 361(2020), p. 455.

[12] Q. Wang, S.Y. Jia, F.G. Tan, G.Q. Li, D.G. Ouyang, S.H. Zhu, W. Sun, and Z. He, Numerical study on desulfurization behavior during kanbara reactor hot metal treatment, *Metall. Mater. Trans. B*, 52(2021), No. 2, p. 1085.

[13] T. Xu, G. Song, Y. Yang, P.X. Ge, and L.X. Tang, Visualization and simulation of steel metallurgy processes, *Int. J. Miner. Metall. Mater.*, 28(2021), No. 8, p. 1387.

[14] V.V. Visuri, T. Vuolio, T. Haas, and T. Fabritius, A review of modeling hot metal desulfurization, *Steel Res. Int.*, 91(2020), No. 4, art. No. 1900454.

[15] Y.J. Lee and K.W. Yi, Improvement of desulfurization efficiency via numerical simulation analysis of transport phenomena of kanbara reactor process, *Met. Mater. Int.*, (2021). DOI: 10.1007/s12540-021-00973-0

[16] D. Lindström and S.C. Du, Kinetic study on desulfurization of hot metal using CaO and CaC_2, *Metall. Mater. Trans. B*, 46(2015), No. 1, p. 83.

[17] T. Mitsuo, T. Shōji, Y. Hatta, H. Ono, H. Mori, and T. Kai, Improvement of desulfurization by addition of aluminum to hot metal in the lime injection process, *Trans. Jpn. Inst. Met.*, 23(1982), No. 12, p. 768.

[18] J.H. Ji, R.Q. Liang, and J.C. He, Numerical simulation on bubble behavior of disintegration and dispersion in stirring-injection magnesium desulfurization process, *ISIJ Int.*, 57(2017), No. 3, p. 453.

[19] K. Feng, A.J. Xu, D.F. He, and L.Z. Yang, Case-based reasoning method based on mechanistic model correction for predicting endpoint sulphur content of molten iron in KR desulphurization, *Ironmaking Steelmaking*, 47(2020), No. 7, p. 799.

[20] F. Oeters, Kinetic treatment of chemical reactions in emulsion metallurgy, *Steel Res.*, 56(1985), No. 2, p. 69.

[21] K. Nakanishi, N. Bessho, Y. Takada, A. Ejima, M. Kuga, J. Katsuki, and M. Kawana, On the desulfurization of the molten metal in an open ladle stirred by an impeller modified by gas injection, *Tetsu-to-Hagané*, 64(1978), No. 10, p. 1528.

[22] W. Chen, Y. Ren, and L.F. Zhang, Large eddy simulation on the two-phase flow in a water model of continuous casting strand with gas injection, *Steel Res. Int.*, 90(2019), No. 4, art. No. 1800287.

[23] W. Chen, Y. Ren, L.F. Zhang, and P.R. Scheller, Numerical simulation of steel and argon gas two-phase flow in continuous casting using LES + VOF + DPM model, *JOM*, 71(2019), No. 3, p. 1158.

[24] W. Chen and L.F. Zhang, Effects of interphase forces on multiphase flow and bubble distribution in continuous casting strands, *Metall. Mater. Trans. B*, 52(2021), No. 1, p. 528.

[25] W. Chen, L.F. Zhang, Y.D. Wang, S. Ji, Y. Ren, and W. Yang, Mathematical simulation of two-phase flow and slag entrainment during steel bloom continuous casting, *Powder Technol.*, 390(2021), p. 539.

[26] F. Oeters, P. Strohmenger, and W. Pluschkell, Kinetik der entschwefelung von roheisenschmelzen mit kalk und erdgas, *Arch. Eisenhüttenwesen*, 44(1973), No. 10, p. 727.

[27] Y. Sano, N. Yamaguchi, and T. Adachi, Mass transfer coefficients for suspended particles in agitated vessels and bubble columns, *J. Chem. Eng. Jpn.*, 7(1974), No. 4, p. 255.

[28] S. Asai, M. Kawachi, and I. Muchi, Mass transfer rate in ladle refining processes, [in] *Proceedings of the Proceedings - SCANINJECT 3, 3rd International Conference on Refining of Iron and Steel by Powder Injection*, Lulea, 1983, p. 1.

[29] H. Lachmund, Y.K. Xie, T. Buhles, and W. Pluschkell, Slag emulsification during liquid steel desulphurisation by gas injection into the ladle, *Steel Res. Int.*, 74(2003), No. 2, p. 77.